The Marine Carbon Footprint: Challenges in the Quantification of the CO₂ Uptake by the Biological Carbon Pump in the Benguela Upwelling System

Tim Rixen, Niko Lahajnar, Tarron Lamont, Rolf Koppelmann, Bettina Martin, Luisa Meiritz, Claire Siddiqui, and Anja K. Van derPlas

Abstract

Quantifying greenhouse gas (GHG) emissions is essential for mitigating global warming, and has become the task of individual countries assigned to the Paris agreement in the form of National Greenhouse Gas Inventory Reports (NIR). The NIR informs on GHG emissions and removals over national territory encompassing the 200-mile Exclusive Economic Zone (EEZ). However, apart from only a few countries, who have begun to report on coastal ecosystems, mostly mangroves, salt marshes, and seagrass meadows, the NIR does not cover

T. Rixen (✉)
Leibniz Centre for Tropical Marine Research - ZMT, Bremen, Germany

Institute of Geology, Universität Hamburg, Hamburg, Germany
e-mail: Tim.Rixen@leibniz-zmt.de

N. Lahajnar · L. Meiritz
Institute of Geology, Universität Hamburg, Hamburg, Germany

T. Lamont
Oceans & Coasts Research Branch, Department of Forestry, Fisheries, and the Environment, Cape Town, South Africa

Department of Oceanography, University of Cape Town, Rondebosch, South Africa

Bayworld Centre for Research & Education, Cape Town, South Africa

R. Koppelmann · B. Martin
Institute of Marine Ecosystem and Fishery Science, Universität Hamburg, Hamburg, Germany

C. Siddiqui
Leibniz Centre for Tropical Marine Research - ZMT, Bremen, Germany

A. K. Van der Plas
National Marine Information and Research Centre, Ministry of Fisheries and Marine Resources, Swakopmund, Namibia

or report on GHG sources and sinks of the 200-mile exclusive economic zone which, for Namibia and South Africa includes the Benguela Upwelling System (BUS). Based on our results, we estimated a CO_2 uptake by the biological carbon pump of 18.5 ± 3.3 Tg C year^{-1} and 6.0 ± 5.0 Tg C year^{-1} for the Namibian and South African parts of the BUS, respectively. Even though it is assumed that the biological carbon pump already responds to global change and fisheries, uncertainties associated with estimates of the CO_2 uptake by the biological carbon pump are still large and hamper a thorough quantification of human impacts on the biological carbon pump. Despite these uncertainties, it is suggested to include parameters such as preformed nutrient supply, carbon export rates, Redfield ratios, and CO_2 concentrations measured at specific key sites into the NIR to stay focussed on the biological carbon pump and to support research addressing open questions, as well as to improve methods and observing concepts.

25.1 Introduction

The implementation of the Paris agreement to keep global warming below 1.5–2.0 °C is accompanied by a variety of measures such as the compilation of the NIR to monitor the emission of CO_2 and other greenhouse gases in order to review the realization of climate pledges at national levels (e.g. UNEP 2019). The National Greenhouse Gas Inventory Report (NIR) splits CO_2 emissions into four sectors: (I) energy, (II) industrial process and product use (IPPU), (III) waste, as well as (IV) agriculture, forestry, and other land use (AFOLU). In order to achieve a comparability of greenhouse gas emissions among different countries, the IPCC provides guidelines to quantify greenhouse gas emissions within these sectors (IPCC 2006). According to the South African, Namibian, and German NIR's the first three sectors are net sources of CO_2, while AFOLU acts as a CO_2 sink to the atmosphere in all three countries (Table 25.1, German Environment Agency 2020; Department of Environmental Affairs 2019; Government of Namibia 2021).

AFOLU quantifies CO_2 emissions caused by land use and land cover changes and is based on the quantification of net changes in carbon stocks. It considers six land-use categories. Among them are wetlands including also coastal ecosystems such as

Table 25.1 CO_2 Emissions from South Africa, Namibia, and Germany according to the NIRs of these countries

Country	South Africa	Namibia	Germany
Reference year	2015	2015	2017
	(Tg C year^{-1})	(Tg C year^{-1})	(Tg C year^{-1})
Total CO_2 emissions	117.6	−29.6	213.0
Sector (I–III)	125.2	1.0	221.4
AFOLU	−7.5	−30.6	−8.4

mangrove forests, tidal marshes, and seagrass meadows (IPCC 2014). Carbon stocks of these coastal wetland reservoirs are named 'blue carbon' due to the colour of the ocean (e.g. Nellemann et al. 2009). Despite being linked by name to the marine environment, blue carbon ignores the CO_2 uptake by phytoplankton and its storage within the ocean's biological carbon pump.

In terms of carbon fixation, phytoplankton in the ocean are as productive as terrestrial plants with a global rate of about 50 Pg C year^{-1} (Field et al. 1998), but the storage of carbon differs in systems dominated by terrestrial plants and marine phytoplankton. Terrestrial plants are the world's largest reservoir of living biomass with a reservoir size of 450 Pg C, whereas phytoplankton represent, with 1–2 Pg C, a relatively small carbon stock (Bar-On et al. 2018; Falkowski et al. 1998). Instead of building-up a huge biomass, carbon fixed by phytoplankton is exported into the deep ocean where the vast majority of the exported biomass is respired and stored as dissolved inorganic carbon (DIC). This results in a strong gradient between low DIC concentrations in surface waters where carbon is fixed via photosynthesis into biomass, and high DIC concentrations at greater depth where the exported organic matter is remineralized. The transfer of DIC into the deep sea favours the CO_2 uptake by the ocean by decreasing the CO_2 concentration and therewith the partial pressure of CO_2 (pCO_2) in surface waters. A hypothetical collapse of the biological carbon pump is assumed to increase the atmospheric CO_2 concentrations by 200–300 ppm, representing a doubling of the pre-industrial atmospheric CO_2 concentration (Heinze et al. 2015).

The CO_2 uptake efficiency of the biological carbon pump is linked to the global thermohaline circulation of the ocean (Heinze et al. 1991; Tschumi et al. 2011) and believed to have played a significant role in controlling atmospheric CO_2 concentrations during glacial/interglacial transitions (Broecker and Barker 2007; Bauska et al. 2016; Schmitt et al. 2012). Even though it is widely assumed that the biological carbon pump also responds to the current climate change (e.g. Laufkötter et al. 2017; Duce et al. 2008; DeVries and Deutsch 2014; Riebesell et al. 2007) and fisheries (Bianchi et al. 2021), neither the magnitude nor the direction of change is predictable (Passow and Carlson 2012; Laufkötter et al. 2017; Laufkötter and Gruber 2018). Considering their potential impact on the CO_2 concentration in the atmosphere and the Paris goals, it appears as a necessity to strongly reduce these uncertainties. This means that variations of the CO_2 uptake by the biological carbon pump should be quantified and respective drivers should be identified, which, in turn, provides background to the discussion on responsibilities (national versus the international community). Here we use data obtained within the BMBF (Federal German Ministry for Education and Research) funded project TRAFFIC (Trophic tRAnsfer eFFICiency) to develop concepts that help to describe the status of the biological carbon pump and to quantify changes of the CO_2 uptake within the BUS.

25.2   Study Area: The Benguela Upwelling System

The BUS stretches from the Angola Benguela Frontal Zone (ABFZ) at ~15°S to Cape Agulhas (~35°S, Fig. 25.1). The south-easterly trade winds emanating from the interplay between the South Atlantic Anticyclone and the continental low-pressure trough, cause the emergence of distinct upwelling cells along the coast (e.g. Kämpf and Chapman 2016; Veitch et al. 2009; Shannon and Nelson 1996). The Lüderitz Upwelling Cell at 26°40′S is the strongest of these cells and divides the BUS into a northern (NBUS) and southern (SBUS) subsystem (e.g. Hutchings et al. 2009; Duncombe Rae 2005; Shannon 1985).

Sub-Antarctic Mode Water mainly feeds upwelling (Marinov et al. 2006; Sarmiento et al. 2004), but its properties vary due to regional differences at sites of its formation and mixing with other water masses. The South Atlantic Central Water (SACW) is comprised of Sub-Antarctic Mode Water that originates as mixture of mainly Antarctic Intermediate Water and Subtropical Mode Water (Souza et al. 2018; Karstensen and Quadfasel 2002; McCartney 1977). It is subducted beneath subtropical surface waters north of the Sub-Antarctic Front at about 36°S–54°S and is fed via the South Atlantic Current into the Benguela Current (e.g. Gordon 1981; Donners et al. 2005). In the southern part of the SBUS, the Benguela Current follows the shelf break towards the equator, while the Benguela Jet, also known as the Cape Jet, flushes the SBUS shelf and carries Indian Ocean Central Water into the SBUS (Durgadoo et al. 2017; Tim et al. 2015). The mixture between South Atlantic Central Water and Indian Ocean water creates a new water mass, which is referred to as the Eastern South Atlantic Water (ESACW, e.g. Liu and Tanhua 2021). The ESACW as well as the SACW which largely encompasses the SBUS along with the Benguela Current, feed the complex equatorial current system. It comprises a number of east- and westward flowing currents and undercurrents (e.g. Pitcher et al. 2021) and finally feed the Angola Current from where modified SACW enters the NBUS as a poleward undercurrent at the ABFZ (Fig. 25.1). During its voyage through the south and equatorial Atlantic Ocean the SACW gets enriched in nutrients and depleted in oxygen (Mohrholz et al. 2008).

South of Lüderitz, the interplay between the Benguela Current, the Benguela Jet, and coastal upwelling creates a complex and temporally varying frontal system starting with the Oceanic Front (e.g. Veitch et al. 2010; Hardman-Mountford et al. 2003). This front is considered as the outer boundary of the SBUS (Barange and Pillar 1992; Shannon and Nelson 1996) whereas the Shelf Break Front and Upwelling Front develop in response to the variable nature of upwelling across the wide shelf regions (Shannon 1985).

During the last two decades, satellite data indicate no significant trends in productivity (Demarcq 2009; Lamont et al. 2019; Verheye et al. 2016), although
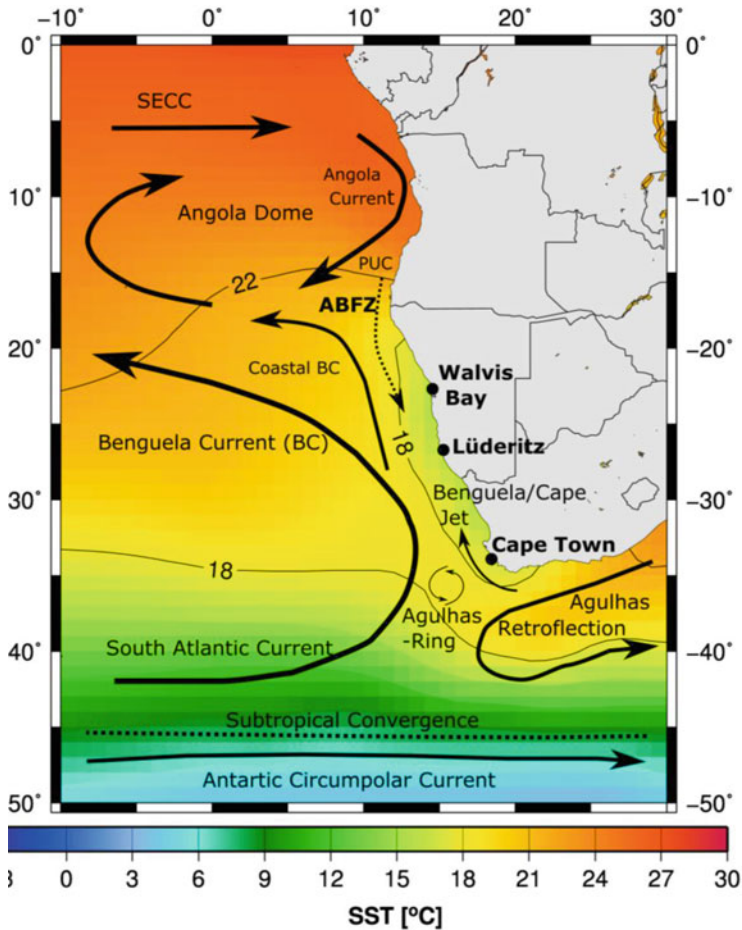
Fig. 25.1 Southeast Atlantic Ocean with its main currents as adopted and simplified from Verheye et al. (2016) and Hardman-Mountford et al. (2003) as well as annual mean sea surface temperatures (Smith et al. 2008). ABFZ (Angola Benguela Frontal Zone) and 'Subtropical Convergence' (dotted line) mark major oceanographic fronts. SECC South Equatorial Counter Current, PUC Poleward Under Current

there is a tendency towards an intensification of upwelling in the SBUS (Lamont et al. 2018, 2019; Tim et al. 2015; Wang et al. 2015; Sydeman et al. 2014). Associated with this trend are shifts in the ecosystem structure such as an overall decrease in zooplankton abundance and a shift from larger to smaller zooplankton species (Lamont et al. 2019; Verheye et al. 2016; Jarre et al. 2015; Hutchings et al. 2012).

25.3   Background

25.3.1 Nutrient Recycling and Productivity

The recycling efficiency of nutrients strongly influences the productivity whereas in general one can distinguish between two different nutrient recycling machineries in pelagic ecosystems. One recycling machinery operates in the seasonal thermocline, while the other one is located in the sunlit surface ocean (euphotic zone) where it directly affects primary production. Eppley and Peterson (1979) divided primary production (CO_2 fixation via photosynthesis) into new and regenerated production. Upwelled nutrients impel new production, while the recycling of nutrients which have been introduced from the dark deep ocean into the euphotic zone fuels the regenerated production. The ratio between new production and primary production defines the f-ratio. An increasing f-ratio indicates a higher contribution of new production to the primary production and hence, a less efficient recycling of nutrients in the euphotic zone. Vice versa, a decreasing f-ratio reflects an enhanced regenerated production and thus a more intense recycling of nutrients. Nevertheless, nutrient recycling does not prevent the loss of nutrients via the export of organic matter from the euphotic zone. Over an annual cycle this so-called export production is assumed to equal new production. Even though export production represents a loss of nutrients from the euphotic zone, the exported organically bound nutrients are not necessarily lost to the pelagic ecosystem as export production drives a secondary recycling machinery in the seasonal thermocline.

The seasonal thermocline defines the subsurface layer from which water is introduced into the euphotic zone on the seasonal times scale which means that the more exported organic matter is remineralized within this subsurface layer, the more formerly exported nutrients return into the euphotic zone and can be recycled (Rixen et al. 2019a). In a coastal upwelling system which is characterized by onshore flowing subsurface waters (upwelling source waters), upwelling at the coast and offshore flowing surface waters, the secondary recycling machinery is part of the nutrient trapping system provoking new production by increasing nutrient concentrations in the upwelling source waters (Dittmar and Birkicht 2001; Tyrrell and Lucas 2002; e.g. Barange and Pillar 1992; Flynn et al. 2020; Rixen et al. 2021). Hereby, the utilization of upwelled nutrients and the associated development of plankton blooms in the offshore flowing upwelled waters initiate the nutrient trapping by exporting the formerly upwelled and now organically bound nutrients into the subsurface waters. This reduces their advection into the open ocean along with offshore flowing surface waters and keeps them within the upwelling system. Although these nutrients increase new production they come from the remineralization of organic matter as those nutrients which drive the regenerated production in the euphotic zone. Hence, these subsurface nutrients are also called regenerated nutrients. Since in addition to nutrients, CO_2 is also released during the remineralization of organic matter, primary production driven by the utilization of regenerated nutrients consumes the associated regenerated CO_2 and creates no need for additional CO_2 as long as the Redfield carbon to nutrient uptake and

remineralization ratio is constant. Hence, even though recycling of nutrients in the euphotic zone and the seasonal thermocline contributes to an elevated productivity of upwelling systems through their impact on regenerated and new production, respectively, it hardly affects the CO_2 storage of the biological carbon pump. This differs with the utilization of preformed nutrients.

25.3.2 Preformed Nutrients and the CO_2 Uptake Efficiency of Biological Carbon Pump

In contrast to regenerated nutrients which are released during the remineralization of exported organic matter, physical processes carry preformed nutrients into the deep ocean. This also occurs during the Sub-Antarctic Mode Water formation in winter when the lack of light prevents the utilization of regenerated nutrients in surface waters. During the subduction of mode water, the biologically unused preformed nutrients are transported into the deep ocean (Knox and McElroy 1984; Sarmiento and Toggweiler 1984; Siegenthaler and Wenk 1984; Duteil et al. 2012; Ito and Follows 2005). The regenerated CO_2 formerly associated with the regenerated nutrients, is, in turn, released from the biological carbon pump. Vice versa, the biological carbon pump takes up CO_2 by the utilization of preformed nutrients and their retransformation into regenerated nutrients at sites such as the BUS where upwelling introduces mode waters into the euphotic zone. To which extent the CO_2 release and uptake affects the CO_2 flux across the air–sea interface depends on its influence on the solubility pump. It could absorb CO_2 released from the biological carbon pump or favour its emission into the atmosphere.

25.3.3 Solubility Pump and Upwelling from a Carbon Cycling Perspective

The solubility pump is an abiotically driven carbon pump which responds to the partial pressure difference of CO_2 (ΔpCO_2) between the surface ocean and the atmosphere. The net flux of CO_2 follows the pressure gradient, which means that CO_2 invades the ocean if the pCO_2 in the atmosphere exceeds the oceanic pCO_2 and vice versa the ocean emits CO_2 into the atmosphere if the pCO_2 in the ocean is higher than it is in the atmosphere. The CO_2 concentration and its temperature- and salinity-controlled solubility determines the pCO_2 in the ocean (Weiss 1974). Hence, CO_2 concentrations link the biological carbon pump and the solubility pump, which gains strength in cold waters due to an increased solubility of CO_2 at low temperatures. If, for example, ocean currents carry warm tropical waters with a pCO_2 exceeding those in the atmosphere into polar regions, the pCO_2 could fall below those in the atmosphere. Consequently, the water takes up CO_2, simply due to decreasing sea surface temperatures. Vice versa, if water masses which are formed in the Southern Ocean such as the SACW, upwell in the BUS, they warm up and release CO_2 that was previously taken up in the Southern Ocean. Hence,

the opposing impacts of the biological carbon pump and the solubility pump on the CO_2 concentrations during the Sub-Antarctic Mode Water formation and upwelling of mode waters in the BUS are parts of one system.

25.4   Data and Methods

In order to study the biological carbon pump within the framework of TRAFFIC, two cruises were carried out with the German research vessels *Meteor* (M153: February, 19th–March 31st 2019) and *Sonne* (SO285: August 20th–November 2nd 2021, Fig. 25.2). Mooring operations were additionally carried out during the *RV Sonne* cruise SO283, the *RS Algoa* cruise ALG 269, and other pre-TRAFFIC cruises with the German RVs *Meteor* and *M.S. Merian*. In addition to sediment trap samples, we analysed water samples to characterize source water masses and the chemical composition of plankton. This allows us to quantify the supply and utilization of preformed nutrients as well as Redfield ratios, which are crucial to translate nutrient consumption into carbon uptake. Furthermore, satellite data were evaluated and linked to sediment trap data in order to estimate the reliability of export production rates. Satellite-derived sea surface temperature (SST) and primary production rates (PP) were downloaded from the MODIS-Aqua website in August 2021 (https://oceandata.sci.gsfc.nasa.gov/MODIS-Aqua/Mapped/Monthly/4km/sst/) and the ocean primary production website in August 2020 (http://www.science.oregonstate.edu/ocean.productivity/).

25.4.1 Particulate Matter

Particulate matter was collected by moored and drifting sediment traps, as well as through the filtration of water samples and by net catches.

A sediment trap mooring was deployed off Walvis Bay (14.04°E/23.02°S) and equipped with a Hydrobios MST-12 sediment trap at water-depths between 65 m and 75 m (~74 m above the sea floor). Since the moored TRAFFIC traps have yet not fully been recovered, we focus on the pre-TRAFFIC deployment periods. This includes seven deployment periods, which are in part not time-coherent. The first deployment started in December 2009 and the last deployment ended in November 2017. Furthermore, four short-term drifting sediment trap systems were deployed in the NBUS and SBUS for about 41–83 h during the cruise M153 (Fig. 25.2). These systems were equipped with four to five single sediment traps and a Hydrobios MST-12 trap at the bottom of the drifter at water-depths of down to 500 m. In total, 24 drifter samples were collected and analysed in Germany.

According to common sediment trap processing procedures, sediment trap samples were split into fractions of >1 mm and <1 mm (Haake et al. 1993; Honjo et al. 2008). The >1 mm fraction contained larger swimmers and the <1 mm fraction was assumed to represent the gravitationally driven export of particles (= particle flux). In addition, the 24 drifter samples were additionally macroscopically
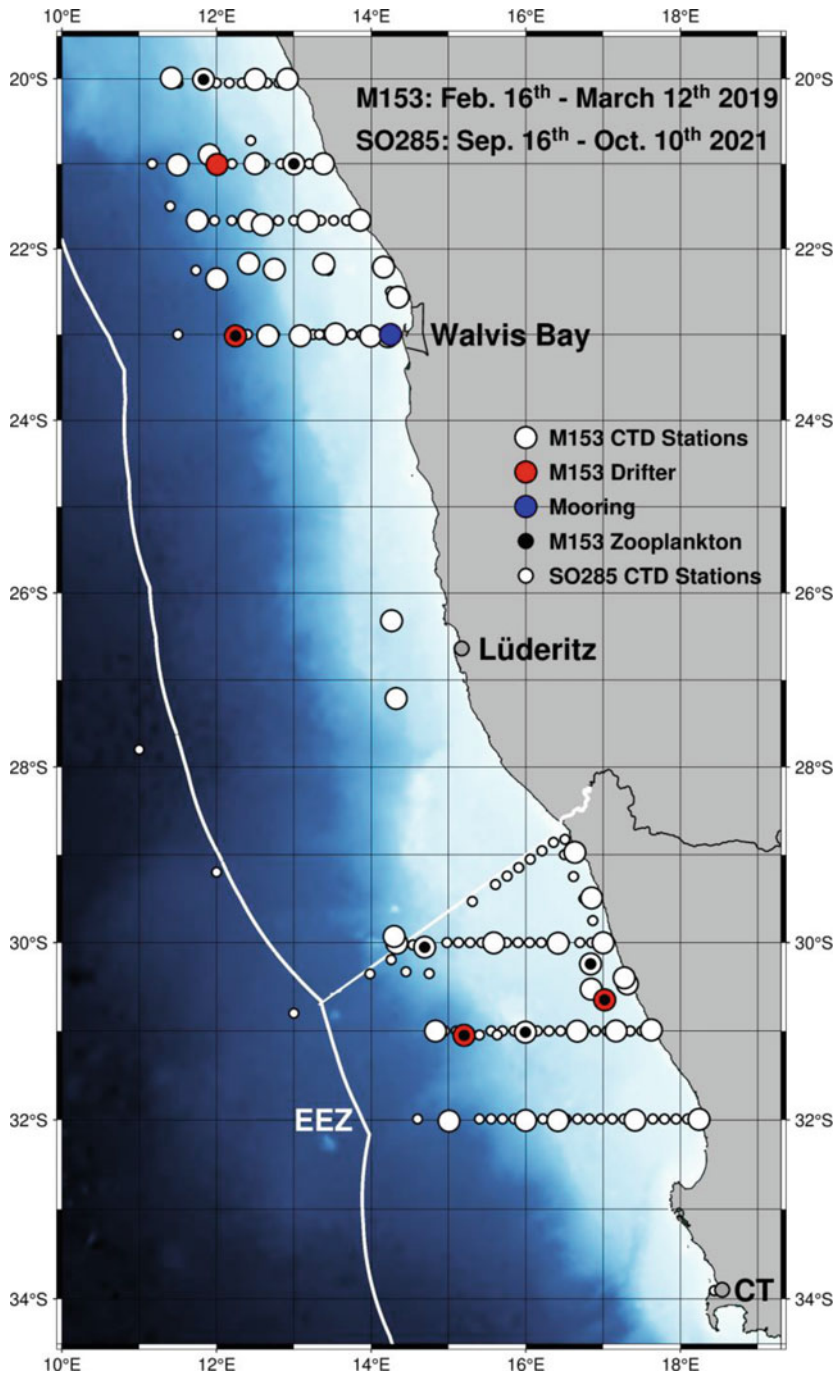
Fig. 25.2 Working area and sampling sites during the two TRAFFIC cruises M153 and SO285. EEZ = 200-mile Exclusive Economic Zones, CT indicates Cape Town. Please note that the timing of the cruises indicates the time within the working area

and microscopically examined and the picked zooplankton was divided into three genera, namely copepods, amphipods, and euphausiids. Furthermore, we obtained zooplankton and fish samples from net catches at the deployment stations during the cruise M153 (Fig. 25.2). These samples were fully homogenized and analysed.

Water samples (5 L and 30 L) obtained from the CTD rosette water sampler were filtered (WHATMAN GF/F; ~0.7 μm; 47 mm diameter) and rinsed with deionized water. Subsequently, filters were dried, shipped to Germany, and analysed in accordance to the sediment trap samples. A detailed description of the sediment trap sample procedure including the biogeochemical analysis is given by Haake et al. (1993) and Rixen et al. (1996). The analysis included the determination of total carbon and nitrogen and organic carbon. The phosphorus content was additionally determined in zooplankton samples according to a method modified from Aspila et al. (1976) and Grasshoff et al. (1999).

25.4.2 Water Sampling

The profiling *Seabird Electronics* (SBE) 911plus CTD system was equipped with a *Digiquartz* pressure sensor, a SBE3 temperature and SBE4 conductivity sensor within a double sensor setup, and a SBE43 dissolved oxygen sensor. Additionally, water samples were taken from the CTD rosette water sampler to analyse DIC concentrations as well as the total alkalinity (TA) and nutrient concentrations. Therefore, we used a cavity ringdown spectrometer (*Picarro* G2201-I, 1510CFIDS2047_v1.0) attached to a Liaison A0301 (DIC), a VINDTA 2C analyser (MARIANDA, Kiel, Germany, TA), and a continuous flow injection system (*Skalar San plus System*). Detection limits for nitrate/nitrite (NO_x) and phosphate were 0.08 μM and 0.07 μM, respectively (Flohr et al. 2014). Both the *Picarro* and the VINDTA 2C analyser were calibrated using Certified Reference Material (CRM, batch #177) provided by A. Dickson (Scripps Institution of Oceanography, La Jolla, CA, USA). The accuracy was ±12 μmol kg^{-1} and ± 4.3 μmol kg^{-1} for DIC and TA, respectively.

25.5 Results and Discussion

25.5.1 CO_2 Concentrations

Within the BUS, CO_2 concentrations were high in a narrow belt along the coast (Emeis et al. 2018) where ESACW and SACW enriched in nutrients and CO_2 reach the surface. Plankton blooms developing in response to the nutrient input consume nutrients and CO_2. Thereby they decrease the concentration of both components in the offshore flowing surface water until nitrate is consumed and phosphate concentrations drop to values of ~0.2 μmol kg^{-1} (Flohr et al. 2014). This so-called excess phosphate is assumed to be the result of a nutrient uptake which follows the Redfield ratio and a relative enrichment of phosphate over nitrate due to anaerobic

processes within the Oxygen Minimum Zone (OMZ) on the shelf and surface sediments (Flohr et al. 2014; Mashifane 2021; Nagel et al. 2013; Goldhammer et al. 2010). However, after the consumption of nitrate within offshore flowing surface waters, a balance between nitrate consumption and release during the respiration of organic matter prevents nitrate accumulation in the euphotic zone. Since such a regenerated nutrient cycle hardly affects CO_2 concentrations, the variability of pCO_2 is strongly reduced at approximately 340 km from the coast. This can be seen in the BUS (Siddiqui et al. 2023) as well as in the California Upwelling System (Chavez and Messié 2009) and marks in addition to nitrate concentrations below the detection limit, the diminishing influence of upwelling on the pelagic ecosystem. At these outskirts of the upwelling-driven ecosystem, CO_2 concentrations reflect the balance between the CO_2 uptake via the utilization of preformed nutrients (biological carbon pump) and the warming of the upwelling water (solubility pump). Vice versa, changing CO_2 concentrations at such sites indicate varying intensities of these two pumps within the upwelling system. Hence, moored CO_2 observing buoys, including oxygen, nitrate, and pH sensors could help to detect long-term changes in the balance between the biological carbon pump and solubility pump. Since the region influenced by upwelling varies and is fragmented by mesoscale eddies and filaments (e.g. Rubio et al. 2009), it is suggested to deploy such CO_2 observing buoys along transects perpendicular to the coast encompassing the region in which nitrate depletion and low variability of pCO_2 indicate the diminishing effect of upwelling on pelagic ecosystems.

25.5.2 Export Production

Export/new production can be used in conjunction with satellite-derived primary production rates to characterize the recycling efficiency in the euphotic zone as indicated by the f-ratio. Combined with the supply of preformed nutrients along with upwelling source water masses, it is also a parameter that allows us to estimate the CO_2 uptake by the biological carbon pump as we will discuss in the following sections. However, so far there are no reliable methods to measure export production directly. Due to uncertainties involved in methods commonly applied to determine export production, estimates of global mean export production rates reveal a wide range with values between 1.8 and 27.5 Pg C year^{-1} (Lutz et al. 2007; del Giorgio and Duarte 2002; Honjo et al. 2008). A widely accepted global mean export production is centred around 10 Pg C year^{-1} (Emerson 2014: and references therein) resulting in a mean area normalized export production rate of 28 g C m^{-2} year^{-1} (area of the ocean 360 10^{12} m^2) and a global mean f-ratio of 0.2.

25.5.2.1 Export Production: A Top-Down Approach
In contrast to the bottom-up approach in which nutrient concentrations are multiplied by upwelling velocities to quantify new/export production (e.g. Chavez and Messié 2009; Messié et al. 2009; Waldron et al. 2009), other methods address

the issue of export production from a top-down approach by looking at primary production. Thereby, export production is described as a simple function of primary production. Eppley and Peterson (1979) introduced one of the first functions which assumes that export/new production (POC_{Export}) contributes 50% (f-ratio 0.5) to the total primary production (PP) in high productive systems (see Eq. 25.1). Laws et al. (2000) and Henson et al. (2011) additionally considered impacts of sea water temperatures (SST) on the link between export and primary production as shown in Eqs. (25.2) and (25.3).

$$POC_{Export} = \begin{matrix} 0.0025 \cdot PP^2, & \text{if } PP < 200 \\ 0.5 \cdot PP, & \text{if } PP > 200 \end{matrix} \qquad (25.1)$$

$$POC_{Export} = (-0.02 \cdot SST + 0.63) \cdot PP \qquad (25.2)$$

$$POC_{Export} = 0.23 \cdot exp^{(-0.08 \cdot SST)} \cdot PP \qquad (25.3)$$

In the BUS, SSTs vary in general between <20 °C at the ABFZ and about 10 °C at sites where upwelling source waters reach the surface. Within this temperature range, f-ratios (= POC_{Export}/PP) as derived from Eqs. (25.2) and (25.3) are far below 0.5, with means of 0.3 ± 0.06 and 0.07 ± 0.02, respectively (Fig. 25.3). This implies a much stronger nutrient recycling in the euphotic zone and a lower export production at the same primary production. We used these equations in addition to satellite-derived primary production rates and SST to calculate export production rates, which were compared to organic carbon fluxes measured by a sediment trap deployed in the NBUS (Figs. 25.2 and 25.4).

The sediment trap was deployed in a water-depth of 60–75 m close to the Namibian coast within the narrow belt along the coast where CO_2 concentrations and primary production are high. According to satellite data, the mean primary production rate over the period of the sediment trap experiment from 2009 to 2018 was about 3000 mg m^{-2} day^{-1}. This is high, but within the upper range of primary production rates measured in situ during expeditions (Barlow et al. 2009; Wasmund et al. 2005). Export production rates derived from the three equations vary (Eq. 25.1 = 1794 $\pm$ 426 mg m^{-2} day^{-1}; Eq. 25.2 = 1101 $\pm$ 295 mg m^{-2} day^{-1}) due to the different f-ratios, whereas results obtained from Eq. (25.3) (229 $\pm$ 64 mg m^{-2} day^{-1}) are similar to organic carbon fluxes measured by sediments traps (136 $\pm$ 90 mg m^{-2} day^{-1}). However, since the sediment trap was deployed at a water-depth of 60–75 m within the thermocline where exported organic matter is respired as indicated by low oxygen concentrations, trap results do not reflect export production rates but only the export of organic matter at water-depth 60–75 m. Hence, the difference between the export production and the measured organic carbon flux indicates the organic matter remineralization between the base of the euphotic zone and the trap-depth. Data obtained in the SBUS allowed us to study organic matter decomposition at such low water-depths in more detail.
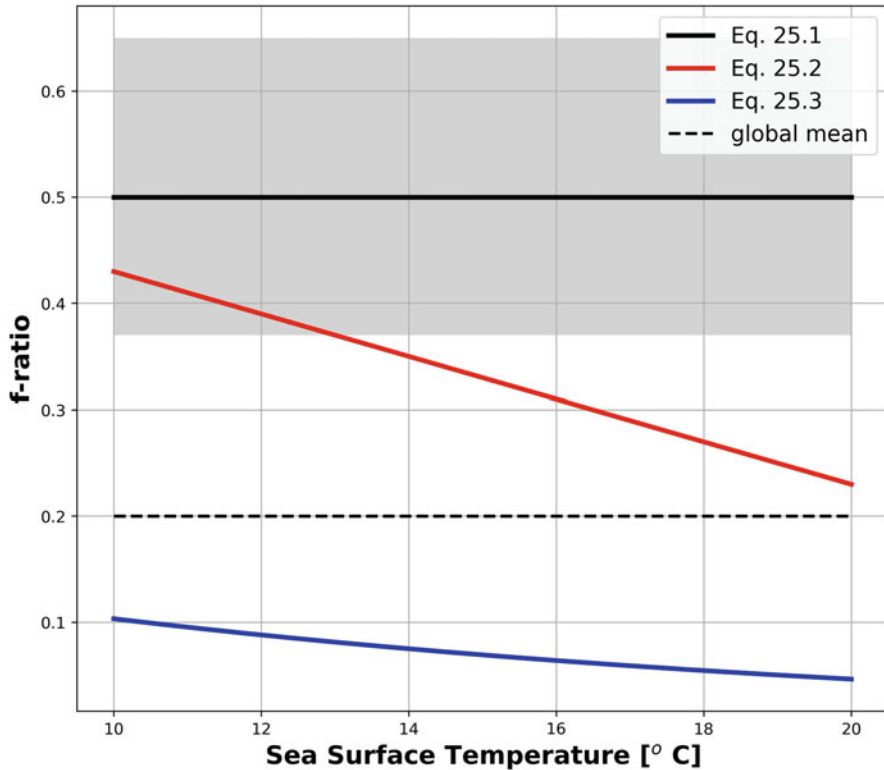
Fig. 25.3 f-ratio versus sea surface temperatures according to Eqs. (25.1), (25.2), and (25.3) as well as in comparison to the global mean f-ratio (dotted line) and those determined by our SBUS drifter study (grey shaded area)

During the cruise M153 (February, 19th–March 31st 2019) a drifter was deployed close to the South African coast, with sediment traps attached at four different water-depths (20, 30, 50, and 75 m) at one of our 24 hour-stations. At this station in situ primary production was also determined by using measured photosynthesis-light-curves (PE curves) in combination with incubation experiments at in situ temperatures and different light intensities. Furthermore, CTD casts were conducted four times a day in order to capture a diurnal cycle and during the cruise SO285 (August 20th–November 2nd 2021) this site was revisited (Fig. 25.5). The drifter traps showed that the total flux of organic carbon was highest just below the surface mixed layer at a water-depth of 20 m (1588 mg m^{-2} day^{-1}) and decreased step-wise with increasing water-depth. At a water-depth of 75 m, the '20 m-flux' had already decreased by 78% to 358 mg m^{-2} day^{-1}. Measured in situ primary production reached values of about 2430 mg m^{-2} day^{-1} and were similar to monthly mean satellite-derived primary production rates of 3428 mg m^{-2} day^{-1} (March, 2019). Primary production of 2430–3428 mg m^{-2} day^{-1} and an export production of
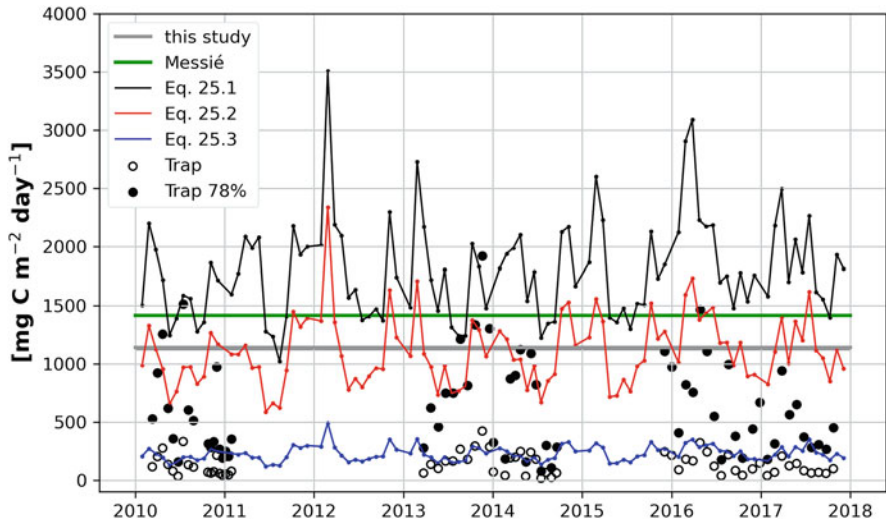
Fig. 25.4 Export production rates derived from Eqs. (25.1)–(25.3) (top-down approaches) as well as from bottom-up approaches (this study and Messié et al. 2009) which are based on upwelling velocity, nutrient concentrations in source waters, and a fixed carbon to nutrient ratio. Open circles indicate organic carbon fluxes measured by moored sediment trap off Walvis Bay in the NBUS at water-depth between 60 m and 74 m (Trap, see Fig. 25.2) while black circles indicate the corrected sediment trap data. The sediment trap data have been corrected for remineralization below the surface mixed layer by assuming that 78% of the exported organic matter is decomposed between the base of the surface mixed layer and the trap (Trap 78%)

1588 mg m^{-2} day^{-1} result in a f-ratio of 0.65 and 0.37, respectively. f-ratios used in Eq. (25.1) and obtained by Eq. (25.2) partly fall in this range whereas f-ratios derived from Eq. (25.3) seem to be too low (Fig. 25.3).

Assuming that 78% of the export production is decomposed between the base of the surface mixed layer and a water-depth of about 75 m implies that the measured mean organic flux of 136 ± 90 mg m^{-2} day^{-1} at our NBUS trap site represents only 78% of the export production which, in turn, suggests an export production of 618 ± 410 mg m^{-2} day^{-1}. If one applies this 78%-correction to all measured sampling intervals, it shows that there are several periods at which the corrected organic carbon export rates are similar to those derived from Eq. (25.1) and partly even Eq. (25.2) (Fig. 25.4). This by far does not solve the dilemma of determining export production rates nor the accuracy of sediment trap measurements, but merely increases the reliability of Eq. (25.1) and (25.2) as well as our drifter experiment.

The revisit of the SBUS drifter site during the cruise SO285 showed that the seasonally varying mixed layer depth is another factor that needs to be considered when comparing shallow water sediment trap results and satellite data. Even though a similar situation was observed during the cruises M153 and SO285 at this site (Fig. 25.5), the comparison of data obtained during these cruises also shows some pronounced differences. For instance, the surface mixed layer was about
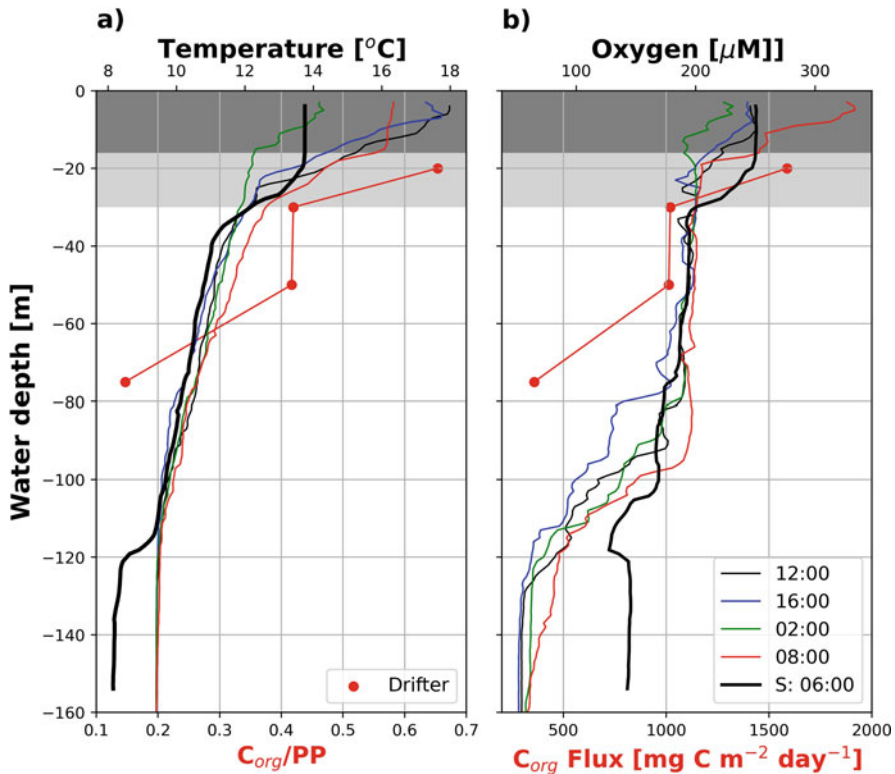
Fig. 25.5 Temperature and oxygen profiles obtained at the near shore drifter site in the SBUS (see Fig. 25.2) at different times of the day during the cruise M153 (March 2019, station 7) and during the cruise SO285 (September/October 2021, station 43) at 06:00 in the morning (S: 6:00). The red circles indicate the ratio between exported organic matter and primary production (C_{org}/PP, a) and organic carbon fluxes determined by the drifter study in four different water-depth. The dark and light grey shades indicate the depth of the surface mixed layer during the cruises M153 and SO285

14 m deeper, while bottom water oxygen concentrations were higher in September 2021 (SO285) than in March 2019 (M153). The intensity of the bottom water OMZ is known to reveal a pronounced seasonal cycle with decreasing oxygen concentrations during the main upwelling season in austral summer and increasing oxygen concentrations during the austral winter (Pitcher et al. 2014). Hence, the bottom water OMZ was more intense in March at the end of the upwelling season than in September at the beginning of the upwelling season. Vertical mixing is, in turn, assumed to supply oxygen to the intermediate water layer so that this layer maintains nearly constant oxygen concentrations over the years. Nevertheless, spatial variations of the Upwelling Front cause temporally limited events during which the oxygen concentration drop by up to ~150 µM (Rixen et al. 2021).

However, the 14 m winter deepening of the surface mixed layer could have strongly influenced results obtained by sediment traps which are deployed at a fixed

water-depth. Assuming a trap-depth of 75 m, a winter deepening of the surface mixed layer by 14 m could have reduced the distance between the trap and the base of surface mixed layer by 30% from 60 m in March to 42 m in September. Considering the rapid decomposition of organic matter as observed in the drifter experiment, such a shortening of the distance between the trap and the base of surface mixed layer should have had a significant impact on the organic carbon fluxes. Hence, measurements of the mixed layer depth should be integrated into shallow water sediment trap studies to correct fluxes for changes in the distance between base of surface mixed layer and the sediment trap. Respective information could, e.g., be obtained by combining sediment trap studies with the deployment of CO_2 observing buoys as discussed before.

25.5.2.2 Export Production: A Bottom-Up Approach

In accordance with Eppley and Peterson (1979) and their Eq. (25.1), Messié et al. (2009) determined with their bottom-up approach a f-ratio of 0.5 for the BUS and f-ratios of 0.4–0.7 for the other eastern boundary upwelling systems. This agrees with results obtained from a comprehensive regional model study suggesting a mean f-ratio of 0.58 (Emeis et al. 2018; Schmidt and Eggert 2016). This regional model was also used to quantify the amount of water (0.9×10^6 m^3 s^{-1}) which upwells in the NBUS off Namibia between 16°S and 28°S (Müller et al. 2014). Following the bottom-up approach we primarily used the M153 and SO285 data to determine the mean nutrient concentrations in the upwelling source waters (Table 25.2), which, subsequently multiplied with upwelling velocities derived from the model, results in the new/export production rate for the BUS.

Table 25.2 Mean properties of the upwelling source water between 18–28°S during the cruises M153 and SO285. Please note that nutrient concentrations have been measured in discrete samples during the cruise M153 and nitrate concentrations by the *SEASCAN SUNA Deep Nitrate Sensor* during the cruise SO285. Other nutrient data from cruise SO285 are not yet available since this cruise was still on-going while this paper was written, n = number of samples and Std = standard deviation

	M153			SO285		
	March, 2019			September, 2021		
	Mean	Std	*N*	Mean	Std	*N*
Density (g cm^{-3})	1.028	0.153	8249	1.028	0.156	9454
Sigma-theta (sθ)	26.69	0.15	8249	25.95	0.16	9454
θ (T$_{pot}$) (°C)	10.36	1.63	8249	10.13	1.77	9454
Salinity	34.93	0.17	8249	33.97	0.20	9454
O$_2$ (μmol kg^{-1})	64.84	33.18	8249	86.29	43.23	9454
NO$_x$ (μmol kg^{-1})	22.59	6.14	141	24.39	4.95	8214
PO$_4$ (μmol kg^{-1})	1.75	0.38	141			
PO$_4$-r (μmol kg^{-1})	1.21	0.36	141			
PO$_4$-p (μmol kg^{-1})	0.53	0.14	141			
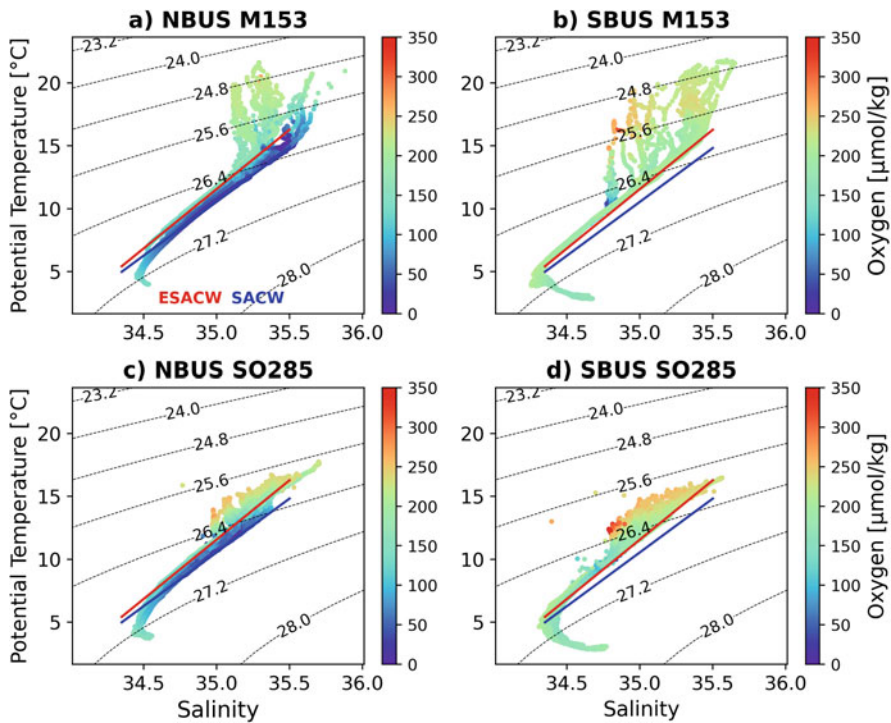
Fig. 25.6 θ-S-diagrams including concentrations of dissolved oxygen derived from CTD casts in NBUS and SBUS during the cruises M153 (February/March 2019) and SO285 (September/October 2021). The red and blue straight lines indicate the θ-S characteristics of the ESACW and SACW according to the equation given by Flohr et al. (2014)

SACW and ESACW, the principal source waters in the BUS, can be identified in θ-S-diagrams as they fall on distinct straight lines within a density range of 27.3 to 26.4 (Fig. 25.6). The comparison between cruises M153 and SO285 shows pronounced differences in the surface water properties. Summer warming decreased the density of surface water and increased the density gradient between surface and upwelling source waters in March, whereas winter cooling had an opposing effect (Fig. 25.6). It decreased the density gradient between surface waters and upwelling source water masses. In contrast to the surface water, the physical properties of upwelling source waters with this density horizon showed hardly any variations except in concentrations of dissolved oxygen (Table 25.2). In the NBUS, they were lower in March than in September due to an enhanced inflow of oxygen-poor SACW between March and May (Mohrholz et al. 2008).

In comparison to oxygen the seasonal variability of nitrate was low (Table 25.2). A mean nitrate concentration of 23.5 μmol kg^{-1} (= (22.59 + 24.39)/2) and a phosphate concentration of 1.75 μmol kg^{-1} multiplied by the mean upwelling velocity of 0.9 $\times$ 10^6 m^3 s^{-1} ($\sim$0.93 $\times$ 10^6 kg s^{-1}) suggest nutrient inputs

into the surface layer of 52.5×10^9 mol phosphate and 718.5×10^9 mole nitrate. Multiplied by a carbon to nitrogen and carbon to phosphorus ratio of 7.6 and 106, which will be discussed in the following sections, these nutrient inputs suggest a new/export production rate of 65–67 Tg C year^{-1}. Considering an area of 0.16×10^{12} m^2 these values imply export production rates of 1113–1147 mg m^{-2} day^{-1} which is within the range of export production rates derived from Eq. 25.2 (1101 ± 295 mg m^{-2} day^{-1}) and below those (1416 mg m^{-2} day^{-1}) obtained by Messié et al. (2009). Multiplied by an area of 0.16×10^{12} m^2 the export production of 1416 mg m^{-2} day^{-1} amounts to 83 Tg C year^{-1} which we will consider as upper estimate for the export production in the BUS between 18°S and 28°S in the following discussion.

25.5.3 Redfield Ratio

In 1934, Redfield introduced the concept of a constant carbon to nutrient ratio in the year 1934 and provided further support in a couple of follow-up publications (e.g. Redfield 1934, 1958; Redfield et al. 1963). He discovered that changes in the concentration of DIC, nitrate, phosphate, and oxygen in the water column reflect the stoichiometry of plankton. Today a C/N/P/-O$_2$ ratio of 106/16/1/−138 is considered as the classical Redfield ratio. During the last 60 years, the number of observations increased enormously showing that the Redfield ratios derived from correlations of dissolved components reveal a remarkably low variability (Anderson and Sarmiento 1994; Takahashi et al. 1985) in comparison to those derived from the elementary composition of plankton (Boyd and Trull 2007; Planavsky 2014; Martiny et al. 2013). Hence, we are again confronted with a discrepancy between bottom-up (dissolved components) and top-down (plankton stoichiometry) approaches.

25.5.3.1 Redfield Ratio: A Top-Down Approach

A main factor controlling the Redfield ratio is the ratio between cyanobacteria and eukaryotic plankton as cyanobacteria often show enhanced and highly variable Redfield ratios (Karl et al. 1997; Bertilsson et al. 2003; Sanudo-Wilhelmy et al. 2004). Hence, C/N/P ratios in oligotrophic subtropical gyres dominated by cyanobacteria are high, with C/N/P values of 195:28:1 (Martiny et al. 2013; Teng et al. 2014). However, in addition to variations in plankton community structure, environmental changes such as temperature and pH variations as well as nutrient stress could influence the carbon to nutrient ratios in individual plankton clades (Boyd and Trull 2007; Planavsky 2014; Martiny et al. 2013; Geider and La Roche 2002; Riebesell et al. 2007). Hence, organic matter in nutrient-rich environments and at high latitudes often reveal lower Redfield ratios (78/13/1, C/N = 6) than in nutrient-depleted regions (138/18/1, C/N = 7.7) at lower latitudes (Martiny et al. 2013; Teng et al. 2014).

This compilation also shows that in comparison to C/P ratios, the variability of C/N ratios is quite low (6–7.7) and hardly deviates from the classical Redfield ratio

Table 25.3 Mean C/N and C/P ratios with corresponding standard deviations (std) and *n* number of samples measured. The samples were obtained from net catches at locations marked as 'M153 Zooplankton' in Fig. 25.2

|	C/N		C/P		n
	Mean	Std	Mean	Std	
Fish	4.6	0.5	61.6	15.6	13
Squid	4.5	0.5	106.8	10.5	5
Zooplankton	5.1	0.7	82.0	11.5	15
Jelly fish	4.0	0.2	110.0	16.3	4

of 6.6. We obtained a similar result from plankton samples which were collected within the chlorophyll maximum during the cruise M153. The chlorophyll maximum is the zone within surface waters where the highest chlorophyll concentration occurs. C/N ratios determined from these samples vary between 5.6 and 8.6, with a mean of about 6.7 in the NBUS and SBUS. Zooplankton, fish, squid, and jelly fish samples collected by net catches during the cruise M153 reveal, in turn, lower C/N ratios of about 4.7 ± 0.7 ($n = 37$), suggesting an enrichment of nitrogen within higher trophic levels of the food web (Table 25.3).

   Our zooplankton samples include euphausiids, amphipods, and decapods, but excluded copepods. Copepods are abundant in the BUS as well as in our drifter samples and are known to reveal highly variable C/N ratios of 3.6–10.4 (Bode et al. 2015; Schukat et al. 2014). In order to study the role of zooplankton in more detail, we also deployed drifting sediment traps during the cruise M153 as mentioned before. The results show that the zooplankton carbon contributes on average $65 \pm 21\%$ to the total organic carbon collected by the traps with a mean C/N ratio of 7.8 ± 1.1. Considering the total organic carbon flux (zooplankton and the <1 mm fractions) results in a mean C/N ratio of 8.1 ± 1.8. This is similar to the mean C/N ratios of 8.7 determined by other sediment trap experiments in the region including traps deployed at water-depths down to 2500 m (Vorrath et al. 2018) and those C/N ratios measured in the moored NBUS traps (8.4 ± 1.3). Compared to phytoplankton (5.6–8.6, mean: 6.7), these slightly enhanced C/N ratios could be caused by a preferential decomposition of organically bound nitrogen in the water column or inputs of organic matter from land and resuspended sediments. On the other hand, we discovered in line with an earlier study along the European continental margin (Antia 2005) a preferential leaching of phosphorus containing organic components, which raised C/P ratios to values of >400. Hence, C/P ratios measured in trap samples have been ignored in this discussion. Along the European continental margin where traps had been deployed at water-depths between 600 and 3200 m, leaching of organically bound nitrogen raised the C/N ratio on average from 8.1 to 11.3 (Antia 2005). Even though a mean C/N ratio of 8.1 ± 1.8 as measured by our traps at a water-depth of 60–75 m implies a comparably low leaching of organically bound nitrogen, it could suffice to explain the slightly enhanced C/N ratio in the trapped exported organic matter. To which extent C/N ratios derived from

concentrations of DIC, phosphate, and nitrate reflect those of particulate matter will be discussed in the next section.

### 25.5.3.2 Redfield Ratio: A Bottom-Up Approach

In the NBUS and SBUS, nitrate and phosphate concentrations are correlated, while the slope derived from the regression equation suggests mean N/P ratios of 13.7–14 (Fig. 25.7). The slightly lower N/P ratio in the NBUS (Fig. 25.7b) is most likely a consequence of nitrate reduction (Tyrrell and Lucas 2002). This occurs in the NBUS OMZ (e.g. Nagel et al. 2013), which is more intense than the SBUS OMZ. However, C/N and C/P ratios are more difficult to determine since the solubility pump accounts for the majority of the carbon dissolved in ocean waters. The y-axis intercept of the regression line derived from the correlation between phosphate and DIC concentrations indicates the DIC background concentrations of 2144 μmol kg^{-1} in the NBUS and 2085 μmol kg^{-1} in SBUS. These differences could be caused by the dissolution of carbonates, as well as varying pCO_2 disequilibria between surface waters and the atmosphere and the uptake of anthropogenic
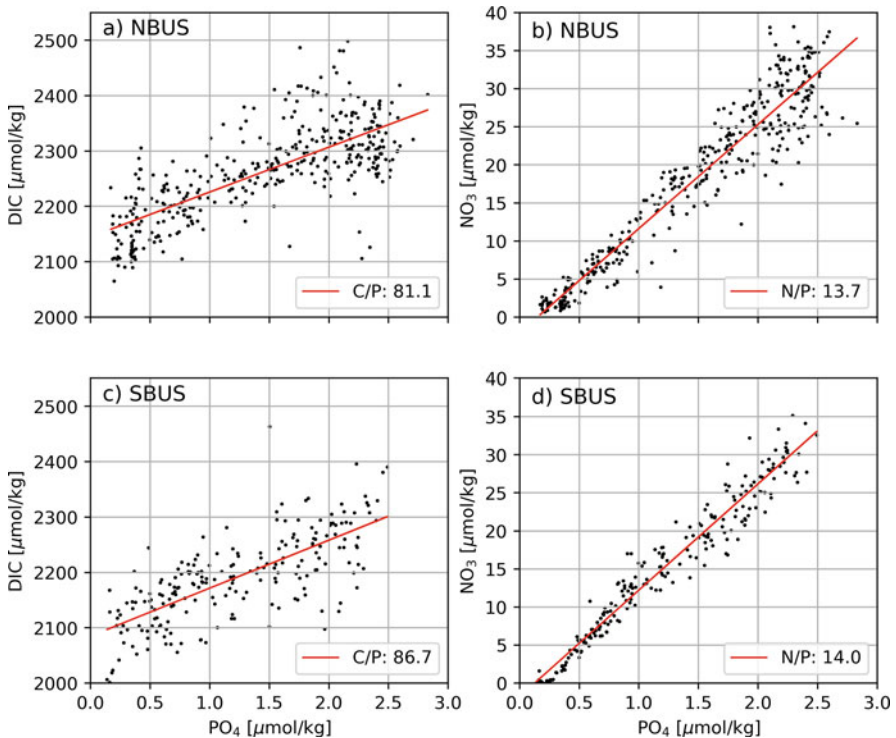
Fig. 25.7 DIC versus phosphate concentrations as well as phosphate versus nitrate concentrations measured in samples obtained in NBUS and SBUS during the cruise M153

CO_2 during the formation of ESACW and SACW. The slopes, in turn indicate C/P ratios of 81.1 and 86.7 in the NBUS and SBUS, respectively.

Well-accepted and often used methods (Sabine et al. 1999; Gruber et al. 2019) associated with the quasi-conservative tracer ΔC^* can be used to quantify the influence of the pCO_2 disequilibria between ocean and atmosphere, the dissolution of carbonate and the uptake of anthropogenic CO_2 on the DIC concentration (Gruber et al. 1996). But since these methods already rely on the assumption of a constant Redfield ratio as derived from Anderson and Sarmiento (1994) of 117/16/1/170 (C/N/P/$-O_2$), they are not applicable here where we aim to determine Redfield ratios in the BUS. Nevertheless, deviation from the minimum TA was considered as a consequence of carbonate dissolution and the corresponding release of DIC ($DIC_{dissolution} = (TA_{measured} - TA_{minimum})/2$) as well as the DIC background concentrations were subtracted from the measured DIC concentrations ($DIC_{corrected} = DIC_{measured} - DIC_{dissolution} - DIC_{background}$). These corrections reduced the differences between NBUS and SBUS, and the slope of the resulting regression equation implied a C/P ratio of 93 (Fig. 25.8). C/P ratios varying between 81.1 and 93.0 combined with N/P ratios of 13.7–14.0 suggest a mean Redfield ratio of $87 \pm 6/14 \pm 0.2/1$. The resulting C/N of about 6.3 falls slightly below the classical Redfield C/N ratio of 6.6 and C/N ratios determined by us in the chlorophyll maximum with a mean of about 6.7. Considering the chlorophyll maximum C/N ratios instead of the N/P ratio derived from nitrate and phosphate concentrations results in a mean Redfield ratio of $87 \pm 6/13 \pm 3/1$. The differences between these two approaches are low and the overall relatively low Redfield ratios are similar to those derived from plankton in nutrient-rich environments and high latitudes
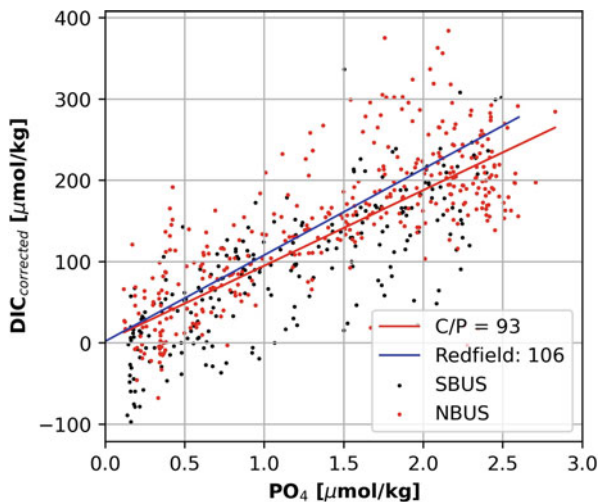
Fig. 25.8 Corrected DIC versus phosphate concentrations from the NBUS and SBUS. The red line marks the regression equation ($DIC_{corrected} = 92.9 \times PO_4 + 2.129$, $r = 0.782$, $n = 617$) and the blue line shows show the Redfield ratio

(78/13/1). However, in February 2011, we determined with a bottom-up approach a Redfield ratio of about $100 \pm 1/16 \pm 2/1$ off Namibia and also located a region on the Namibian shelf where anaerobic processes in association with nutrient fluxes across the sediment water interface reduced the Redfield ratio to 66/10/1 (Flohr et al. 2014). Hence, Redfield ratios seem to vary interannually and could be influenced by sediment water interactions within pronounced bottom water OMZ. Nevertheless, regarding the CO_2 uptake by the biological carbon pump, our bottom-up and top-down approach based on the M153 data support Redfield's findings and imply that the consumption of upwelled nitrate and phosphate adsorbs as much CO_2 as is released during the respiration of exported organic matter. This, in turn, poses the question as to how the carbon export could influence the CO_2 uptake by the biological carbon pump.

25.5.4 CO$_2$ Sequestration

In order to estimate carbon sequestration by the biological carbon pump, we applied the bottom-up approach to calculate export production and used the Redfield ratio to convert phosphate supply into surface waters into carbon export production rates. In principle, this approach is similar to those used by Waldron et al. (2009) for the SBUS but in contrast to Waldron et al. (2009), we used only preformed and not the total nutrient concentrations of the source waters. As discussed before, preformed nutrients have been detached from CO_2 so that their utilization acts as a CO_2 sink. Since the preformed phosphate concentrations contribute about 30% to the total phosphate concentration (Table 25.2), the CO_2 uptake by the biological carbon pump amounts to about one third of the total export production. In the BUS between 18°S and 28°S which approximately covers the Namibian part of the BUS, we estimated a total export production of 65–83 Tg C year^{-1}, whereas Waldron et al. (2009) suggested a total export production of about 7–39 Tg C year^{-1} for the South African part of the BUS. Assuming that utilization of preformed nutrients accounts for 30% of the total export production suggests a CO_2 uptake of 20–25 Tg C year^{-1} (mean = 22.5 ± 2.5 Tg C year^{-1}) in the Namibian part of the BUS and 2–12 Tg C year^{-1} (mean = 7 ± 5 Tg C year^{-1}) in the South African part of the BUS which is similar to the results of our previous study (Siddiqui et al. 2023).

In order to estimate possible impacts of changing Redfield ratio, we repeated the calculations but instead of the classical C/P ratio of 106, we used a C/P ratio of 87 ± 6 as determined by using the M153 data. The resulting effect can be calculated by the rule of three (export driven by preformed nutrients/106 × 87 ± 6) which lowered the mean CO_2 uptake rates to 18.5 ± 3.3 Tg C year^{-1} and 6.0 ± 5.0 Tg C year^{-1} for the Namibian and the South African part of the BUS, respectively. This represents a decrease of the calculated CO_2 uptake by the biological carbon pump of 17% (4 Tg C year^{-1}) and 13% (1 Tg C year^{-1}) off Namibia and South Africa.

The CO_2 uptake rates by the biological carbon pump of 18.5 ± 3.3 Tg C year^{-1} and 6.0 ± 5.0 Tg C year^{-1} are in the same order of magnitude as the CO_2 uptake by AFOLU of 30.6 Tg C year^{-1} (Namibia) and 7.5 Tg C year^{-1} (South Africa, see Table 25.1), but these carbon fluxes cannot be compared to each other since the latter represents human impacts on the CO_2 uptake by terrestrial ecosystems. Even though marine ecosystems respond to global change (Lamont et al. 2019; Verheye et al. 2016; Jarre et al. 2015; Hutchings et al. 2012), fisheries (Bianchi et al. 2021) and in particular bottom trawling which will be discussed in the following section, effects on the CO_2 uptake by the biological carbon pump via influences on the Redfield ratio have not yet been quantified. Nevertheless, the magnitude of the CO_2 uptake rates by the biological carbon pump is on levels at which small changes due to, e.g., decreasing C/P ratios of 17% or 13%, respectively, could influence the CO_2 uptake by AFOLU significantly.

25.5.5 Benthos

So far, we discussed the CO_2 uptake by the biological carbon pump in the water column, but it also influences the burial of carbon in sediments. This represents a removal of carbon from the climate active carbon cycle and humans could favour and reduce it. An enhanced supply of clay and other minerals via dust inputs and river discharges due to soil as well as coastal erosion favours the organic carbon sedimentation by reducing the remineralization of organic matter in the water column and surface sediments mainly by two processes. Firstly, minerals incorporated into particles increase their sinking speed and the resulting accelerated transport of organic matter from the euphotic zone onto the sediments lowers the residence time of organic matter in the water columns and therewith its remineralization (e.g. Rixen et al. 2019b). Secondly, the adsorption of organic matter to mineral surfaces reduces its remineralization in the water column and surface sediments by protecting organic matter against bacterial attacks (e.g. Armstrong et al. 2002; Hedges 1977). Vice versa, bottom water trawling remobilizes the sedimentary organic matter and favours its return into the climate active carbon cycle. Sala et al. (2021) introduced an approach to quantify impacts of bottom trawling on the remobilization of carbon from marine sediments on a global scale. Assuming a continuous bottom trawling, Sala et al. (2021) suggested, for instance, a global long-term sedimentary organic carbon loss of about 158 Tg C year^{-1}, and also broke it down to the BUS where it amounts to about 5 Tg C year^{-1}. In comparison to AFOLU and our estimates of the CO_2 uptake by the biological Compared to AFOLU and our estimates of the CO_2 uptake by the biological carbon pump of about 24 Tg C/year-1 in the entire BUS (NBUS and SBUS), this is a substantial amount. It shows that humans can significantly affect the CO2 uptake of the biological carbon pump which still needs to be quantified.

25.6   Conclusion

In contrast to the often assumed and used constant global mean Redfield ratio, our results indicate varying Redfield ratios whereas the one determined by us during the TRAFFIC cruise M153 ($87 \pm 6/13 \pm 3/1$) is similar to those derived by other studies in nutrient-rich environments and high latitudes (78/13/1). CO_2 uptake by the biological carbon pump based on the supply of preformed nutrients and the Redfield ratio amounts to 18.5 ± 3.3 Tg C year^{-1} and 6.0 ± 5.0 Tg C year^{-1} for the Namibian and South African parts of the BUS, respectively. These uptake rates are on a level at which small changes could influence the CO_2 uptake by AFOLU significantly. Considering the release of sedimentary carbon by bottom trawling and that ecosystems in the BUS respond to global change and fisheries, it is quite likely that humans affect the CO_2 uptake by the biological carbon pump already but uncertainties are still too large to quantify such impacts. Hence, we suggest to improve methods to estimate the supply of preformed nutrients, carbon export rates, and Redfield ratios and expand monitoring strategies by linking established observing methods such as remote sensing and sediment trap studies, and focus on CO_2 observation at the outer rim of the upwelling system. This appears to be a key site to detect long-term changes in the balance between the biological carbon pump and solubility pump. Despite large uncertainties regarding the CO_2 uptake by the biological carbon pump and its influence on the solubility pump, we propose to include parameters such as preformed nutrient supply, carbon export rates, Redfield ratios, and CO_2 concentrations measured at specific key sites into the NIR.

References

Anderson LA, Sarmiento JL (1994) Redfield ratios of remineralization determined by nutrient data analysis. Glob Biogeochem Cycles 8(1):65–80

Antia AN (2005) Solubilization of particles in sediment traps: revising the stoichiometry of mixed layer export. Biogeosciences 2(2):189–204

Armstrong RA, Lee C, Hedges JI et al (2002) A new, mechanistic model for organic carbon fluxes in the ocean: based on the quantitative association of POC with ballast minerals. Deep-Sea Res 49(II):219–236

Aspila KI, Haig A, Chau ASY (1976) A semi-automated method for the determination of inorganic, organic and total phosphate in sediments. Analyst 101:187–97

Barange M, Pillar SC (1992) Cross-shelf circulation, zonation and maintenance mechanisms of Nyctiphanes capensis and Euphausia hanseni (Euphausiacea) in the northern Benguela upwelling system. Cont Shelf Res 12(9):1027–1042

Barlow R, Lamont T, Mitchell-Innes B et al (2009) Primary production in the Benguela ecosystem, 1999 - 2002. Afr J Mar Sci 31(1):97–101

Bar-On YM, Phillips R, Milo R (2018) The biomass distribution on earth. Proc Natl Acad Sci 115(25):6506–6511

Bauska TK, Baggenstos D, Brook EJ et al (2016) Carbon isotopes characterize rapid changes in atmospheric carbon dioxide during the last deglaciation. Proc Natl Acad Sci 113(13):3465

Bertilsson S, Berglund O, Karl DM et al (2003) Elemental composition of marine Prochlorococcus and Synechococcus: implications for the ecological stoichiometry of the sea. Limnol Oceanogr 48(5):1721–1731

Bianchi D, Carozza David A, Galbraith Eric D et al (2021) Estimating global biomass and biogeochemical cycling of marine fish with and without fishing. Sci Adv 7(41):eabd7554

Bode M, Hagen W, Schukat A et al (2015) Feeding strategies of tropical and subtropical calanoid copepods throughout the eastern Atlantic Ocean – latitudinal and bathymetric aspects. Prog Oceanogr 138:268–282

Boyd PW, Trull TW (2007) Understanding the export of biogenic particles in oceanic waters: is there consensus? Prog Oceanogr 72(4):276–312

Broecker W, Barker S (2007) A 190‰ drop in atmosphere's Δ14C during the "mystery interval" (17.5 to 14.5 kyr). Earth Planet Sci Lett 256(1–2):90–99

Chavez FP, Messié M (2009) A comparison of eastern boundary upwelling ecosystems. Prog Oceanogr 83(1-4):80–96

del Giorgio PA, Duarte CM (2002) Respiration in the open ocean. Nature 420(6914):379–384

Demarcq H (2009) Trends in primary production, sea surface temperature and wind in upwelling systems (1998-2007). Prog Oceanogr 83(1-4):376–385

Department of Environmental Affairs, 2019. South Africa's 3rd Biennial Update Report to the United Nations Framework Convention on Climate Change. Department of Environmental Affairs, South Africa, Pretoria. South Africa., p. 234.

DeVries T, Deutsch C (2014) Large-scale variations in the stoichiometry of marine organic matter respiration. Nat Geosci 7(12):890–894

Dittmar T, Birkicht M (2001) Regeneration of nutrients in the northern Benguela upwelling and the Angola-Benguela front areas. S Afr J Sci 97:239–246

Donners J, Drijfhout SS, Hazeleger W (2005) Water mass transformation and subduction in the South Atlantic. J Phys Oceanogr 35(10):1841–1860

Duce RA, LaRoche J, Altieri K et al (2008) Impacts of atmospheric anthropogenic nitrogen on the open ocean. Science 320(5878):893–897

Duncombe Rae CM (2005) A demonstration of the hydrographic partition of the Benguela upwelling ecosystem at 26° 40′S. Afr J Mar Sci 27(3):617–628

Durgadoo JV, Rühs S, Biastoch A et al (2017) Indian Ocean sources of Agulhas leakage. J Geophys Res Oceans. https://doi.org/10.1002/2016JC012676

Duteil O, Koeve W, Oschlies A et al (2012) Preformed and regenerated phosphate in ocean general circulation models: can right total concentrations be wrong? Biogeosciences 9(5):1797–1807

Emeis K, Eggert A, Flohr A et al (2018) Biogeochemical processes and turnover rates in the northern Benguela upwelling system. J Mar Syst 188:63–80

Emerson S (2014) Annual net community production and the biological carbon flux in the ocean. Glob Biogeochem Cycles 28(1):14–28

Eppley RW, Peterson BJ (1979) Particulate organic matter flux and planktonic new production in the deep ocean. Nature 282:677–680

Falkowski PG, Barber RT, Smetacek V (1998) Biogeochemical controls and feedbacks on ocean primary production. Science 281:200–206

Field CB, Behrenfeld MJ, Randerson J et al (1998) Primary productivity of the biosphere: an integration of terrestrial and oceanic components. Science 281:237–240

Flohr A, van der Plas AK, Emeis K-C et al (2014) Spatio-temporal patterns of C: N: P ratios in the northern Benguela upwelling regime. Biogeosciences 11:885–897

Flynn RF, Granger J, Veitch JA et al (2020) On-shelf nutrient trapping enhances the fertility of the southern Benguela upwelling system. J Geophys Res Oceans 125(6):e2019JC015948

Geider RJ, La Roche J (2002) Redfield revisited: variability of C:N:P in marine microalgae and its biochemical basis. Eur J Phycol 37:1–17

German Environment Agency (2020) Submission under the United Nations Framework Convention on Climate Change and the Kyoto Protocol 2020 National Inventory Report for the German Greenhouse Gas Inventory 1990 – 2018, in: Strogies, M., Gniffke, P. (Eds.). Umweltbundesamt, Germany, Dessau-Roßlau, Germany, p. 997.

Goldhammer T, Bruchert V, Ferdelman TG et al (2010) Microbial sequestration of phosphorus in anoxic upwelling sediments. Nat Geosci 3(8):557–561

Gordon AL (1981) South Atlantic thermocline ventilation. Deep Sea Res A 28(11):1239–1264

Government of Namibia, 2021. Fourth Biennial Update Report (BUR4) to the United Nations Framework Convention on Climate Change, Windhoek, Namibia, p. 120.

Grasshoff, Klaus, Klaus Kremling, and Manfred Ehrhardt. 1999. *Methods of seawater analysis* (Wiley-VCH: Weinheim, Germany).

Gruber N, Sarmiento JL, Stocker TF (1996) An improved method for detecting anthropogenic CO2 in the oceans. Global Biogeochem Cycles 10(4):809–837

Gruber N, Clement D, Carter BR et al (2019) The oceanic sink for anthropogenic CO2 from 1994 to 2007. Science 363(6432):1193

Haake B, Ittekkot V, Rixen T et al (1993) Seasonality and interannual variability of particle fluxes to the deep Arabian Sea. Deep Sea Res I 40(7):1323–1344

Hardman-Mountford NJ, Richardson AJ, Agenbag JJ et al (2003) Ocean climate of the South East Atlantic observed from satellite data and wind models. Prog Oceanogr 59(2):181–221

Hedges JI (1977) The association of organic molecules with clay minerals in aqueous solutions. Geochim Cosmochim Acta 41(8):1119–1123

Heinze C, Maier-Reimer E, Winn K (1991) Glacial pCO_2 reduction by the world ocean: experiments with the Hamburg Carbon Cycle Model. Paleoceanography 6(4):395–430

Heinze C, Meyer S, Goris N et al (2015) The ocean carbon sink – impacts, vulnerabilities and challenges. Earth Syst Dynam 6(1):327–358

Henson SA, Sanders R, Madsen E et al (2011) A reduced estimate of the strength of the ocean's biological carbon pump. Geophys Res Lett 38(4):L04606

Honjo S, Manganini SJ, Krishfield RA et al (2008) Particulate organic carbon fluxes to the ocean interior and factors controlling the biological pump: a synthesis of global sediment trap programs since 1983. Prog Oceanogr 76(3):217–285

Hutchings L, van der Lingen CD, Shannon LJ et al (2009) The Benguela current: an ecosystem of four components. Prog Oceanogr 83(1-4):15–32

Hutchings L, Jarre A, Lamont T et al (2012) St Helena Bay (southern Benguela) then and now: muted climate signals, large human impact. Afr J Mar Sci 34(4):559–583

IPCC, 2006. 2006 IPCC Guidelines for National Greenhouse Gas Inventories, Prepared by the National Greenhouse Gas Inventories Programme, in: Eggleston H.S., Buendia L., Miwa K., T., N., K., T. (Eds.). IPCC National Greenhouse Gas Inventories Programme Technical Support Unit, IGES, Japan

IPCC, 2014. 2013 Supplement to the 2006 IPCC Guidelines for National Greenhouse Gas Inventories: Wetlands Methodological Guidance on Lands with Wet and Drained Soils, and Constructed Wetlands for Wastewater Treatment, in: Hiraishi, T., Krug, T., Tanabe, K., Srivastava, N., Baasansuren, J., Fukuda, M., Troxler, T.G. (Eds.). IPCC, Switzerland

Ito T, Follows MJ (2005) Preformed phosphate, soft tissue pump and atmospheric CO_2. J Mar Res 63:813–839

Jarre A, Hutchings L, Kirkman SP et al (2015) Synthesis: climate effects on biodiversity, abundance and distribution of marine organisms in the Benguela. Fish Oceanogr 24(S1):122–149

Kämpf J, Chapman P (2016) The Benguela current upwelling system. In: Kämpf J, Chapman P (eds) Upwelling systems of the world. Springer, Cham. https://doi.org/10.1007/978-3-319-42524-5_7

Karl D, Letelier R, Tupas L et al (1997) The role of nitrogen fixation in biogeochemical cycling in the subtropical North Pacific Ocean. Nature 388:533–538

Karstensen J, Quadfasel D (2002) Formation of southern hemisphere thermocline waters: water mass conversion and subduction. J Phys Oceanogr 32(11):3020–3038

Knox F, McElroy MB (1984) Changes in atmospheric CO2: influence of the marine biota at high latitude. J Geophys Res Atmos 89(D3):4629–4637

Lamont T, García-Reyes M, Bograd SJ et al (2018) Upwelling indices for comparative ecosystem studies: variability in the Benguela upwelling system. J Mar Syst 188:3–16

Lamont T, Barlow RG, Brewin RJW (2019) Long-term trends in phytoplankton chlorophyll a and size structure in the Benguela upwelling system. J Geophys Res Oceans 124:1170–1195

Laufkötter C, Gruber N (2018) Will marine productivity wane? Science 359(6380):1103

Laufkötter C, John JG, Stock CA et al (2017) Temperature and oxygen dependence of the remineralization of organic matter. Glob Biogeochem Cycles 31(7):1038–1050

Laws EA, Falkowski PG, Smith WO et al (2000) Temperature effects on export production in the open ocean. Glob Biogeochem Cycles 14(4):1231–1246

Liu M, Tanhua T (2021) Water masses in the Atlantic Ocean: characteristics and distributions. Ocean Sci 17(2):463–486

Lutz MJ, Caldeira K, Dunbar RB et al (2007) Seasonal rhythms of net primary production and particulate organic carbon flux to depth describe the efficiency of biological pump in the global ocean. J Geophys Res Oceans 112(C10):C10011

Marinov I, Gnanadesikan A, Toggweiler JR et al (2006) The Southern Ocean biogeochemical divide. Nature 441(7096):964–967

Martiny AC, Pham CTA, Primeau FW et al (2013) Strong latitudinal patterns in the elemental ratios of marine plankton and organic matter. Nat Geosci 6:279

Mashifane TB (2021) Denitrification and anammox shift nutrient stoichiometry and the phytoplankton community structure in the Benguela upwelling system. J Geophys Res Oceans 126(8):e2021JC017816

McCartney MS (1977) Subantarctic mode water. In: Angel MV (ed) A voyage of discovery: George Deacon 70th anniversary volume, Supplement to deep-sea research. Pergamon Press, Oxford, pp 103–119

Messié M, Ledesma J, Kolber DD et al (2009) Potential new production estimates in four eastern boundary upwelling ecosystems. Prog Oceanogr 83(1-4):151–158

Mohrholz V, Bartholomaeb CH, van der Plas AK (2008) The seasonal variability of the northern Benguela undercurrent and its relation to the oxygen budget on the shelf. Cont Shelf Res 28(3):424–441

Müller AA, Reason CJ, Schmidt M et al (2014) Computing transport budgets along the shelf and across the shelf edge in the northern Benguela during summer (DJF) and winter (JJA). J Mar Syst 140(Part B(0)):82–91

Nagel B, Emeis K-C, Flohr A et al (2013) N-cycling and balancing of the N-deficit generated in the oxygen minimum zone over the Namibian shelf—an isotope-based approach. J Geophys Res Biogeo 118:361–371

Nellemann, C., Corcoran, E., Duarte, C.M., Valdés, L., De Young, C., Fonseca, L., Grimsditch, G., 2009. Blue Carbon. A Rapid Response Assessment. United Nations Environment Programme, Arendal, Norway, p. 79.

Passow U, Carlson CA (2012) The biological pump in a high CO2 world. Mar Ecol Prog Ser 470:249–271

Pitcher GC, Probyn TA, du Randt A et al (2014) Dynamics of oxygen depletion in the nearshore of a coastal embayment of the southern Benguela upwelling system. J Geophys Res Oceans 119(4):2183–2200

Pitcher GC, Aguirre-Velarde A, Breitburg D et al (2021) System controls of coastal and open ocean oxygen depletion. Prog Oceanogr 197:102613

Planavsky NJ (2014) The elements of marine life. Nat Geosci 7(12):855–856

Redfield AC (1934) On the proportions of organic derivations in sea water and their relation to the composition of plankton. In: Daniel RJ (ed) James Johnstone memorial volume. University Press of Liverpool, Liverpool, pp 176–192

Redfield AC (1958) The biological control of chemical factors in the environment. Am Sci:205–222

Redfield AC, Ketchum BH, Richards FA (1963) The influence of organisms on the composition of sea-water. In: Hitt MN (ed) The sea. Wiley, New York, pp 26–77

Riebesell U, Schulz KG, Bellerby RGJ et al (2007) Enhanced biological carbon consumption in a high CO_2 ocean. Nature 450(7169):545–548

Rixen T, Haake B, Ittekkot V et al (1996) Coupling between SW monsoon-related surface and deep ocean processes as discerned from continuous particle flux measurements and correlated satellite data. J Geophys Res 101(C12):28569–28582

Rixen T, Gaye B, Emeis K-C (2019a) The monsoon, carbon fluxes, and the organic carbon pump in the northern Indian Ocean. Prog Oceanogr 175:24–39

Rixen T, Gaye B, Emeis KC et al (2019b) The ballast effect of lithogenic matter and its influences on the carbon fluxes in the Indian Ocean. Biogeosciences 16(2):485–503

Rixen T, Lahajnar N, Lamont T et al (2021) Oxygen and nutrient trapping in the southern Benguela upwelling system. Front Mar Sci 8:1367

Rubio A, Blanke B, Speich S et al (2009) Mesoscale eddy activity in the southern Benguela upwelling system from satellite altimetry and model data. Prog Oceanogr 83(1):288–295

Sabine CL, Key RM, Johnson KM et al (1999) Anthropogenic CO_2 inventory of the Indian Ocean. Glob Biogeochem Cycles 13(1):179–198

Sala E, Mayorga J, Bradley D et al (2021) Protecting the global ocean for biodiversity, food and climate. Nature 592(7854):397–402

Sanudo-Wilhelmy SA, Tovar-Sanchez A, Fu F-X et al (2004) The impact of surface-absorbed phosphorus on phytoplankton Redfield stoichiometry. Nature 432:897–901

Sarmiento JL, Toggweiler JR (1984) A new model for the role of the oceans in determining atmospheric pCO_2. Nature 308:621–624

Sarmiento JL, Gruber N, Brzezinski MA et al (2004) High-latitude controls of thermocline nutrients and low latitude biological productivity. Nature 427(6969):56–60

Schmidt M, Eggert A (2016) Oxygen cycling in the northern Benguela upwelling system: modelling oxygen sources and sinks. Prog Oceanogr 149:145–173

Schmitt J, Schneider R, Elsig J et al (2012) Carbon isotope constraints on the deglacial CO2 rise from ice cores. Science 336(6082):711–714

Schukat A, Auel H, Teuber L et al (2014) Complex trophic interactions of calanoid copepods in the Benguela upwelling system. J Sea Res 85:186–196

Shannon LV (1985) The Benguela ecosystem 1. Evolution of the Benguela, physical features and processes. In: Barnes M (ed) Oceanography and marine biology. University Press, Aberdeen, pp 105–182

Shannon LV, Nelson G (1996) The Benguela: large scale features and processes and system variability. In: Wefer G, Berger WH, Siedler G et al (eds) The South Atlantic: present and past circulation. Springer, Berlin, pp 163–210

Siddiqui C, Rixen T, Lahajnar N et al (2023) Regional and global impact of CO2 uptake in the Benguela upwelling system through preformed nutrients. Nat Commun 14:2582

Siegenthaler U, Wenk T (1984) Rapid atmospheric CO_2 variations and ocean circulation. Nature 308:624–627

Smith TM, Reynolds RW, Peterson TC et al (2008) Improvements to NOAA's historial merged land-ocean surface temperature analysis (1880 - 2006). J Clim 21:2283–2296

Souza AGQ, Kerr R, Azevedo JLL (2018) On the influence of subtropical mode water on the South Atlantic Ocean. J Mar Syst 185:13–24

Sydeman WJ, García-Reyes M, Schoeman DS et al (2014) Climate change and wind intensification in coastal upwelling ecosystems. Science 345(6192):77

Takahashi T, Broecker WS, Langer S (1985) Redfield ratio based on chemical data from Isopycnal surfaces. J Geophys Res 90(C4):6907–6924

Teng Y-C, Primeau FW, Moore JK et al (2014) Global-scale variations of the ratios of carbon to phosphorus in exported marine organic matter. Nat Geosci 7(12):895–898

Tim N, Zorita E, Hünicke B (2015) Decadal variability and trends of the Benguela upwelling system as simulated in a high-resolution ocean simulation. Ocean Sci 11(3):483–502

Tschumi T, Joos F, Gehlen M et al (2011) Deep ocean ventilation, carbon isotopes, marine sedimentation and the deglacial CO_2 rise. Clim Past 7(3):771–800

Tyrrell T, Lucas MI (2002) Geochemical evidence of denitrification in the Benguela upwelling system. Cont Shelf Res 22(17):2497–2511

UNEP, 2019. Emissions Gap Report 2019. United Nations Environment Programme (UNEP), Nairobi, Kenya, p. 80.

Veitch J, Penven P, Shillington F (2009) The Benguela: a laboratory for comparative modeling studies. Prog Oceanogr 83(1):296–302

Veitch J, Penven P, Shillington F (2010) Modeling equilibrium dynamics of the Benguela Current System. J Phys Oceanogr 40(9):1942–1964

Verheye HM, Lamont T, Huggett JA et al (2016) Plankton productivity of the Benguela Current Large Marine Ecosystem (BCLME). Environ Dev 17:75–92

Vorrath M-E, Lahajnar N, Fischer G et al (2018) Spatiotemporal variation of vertical particle fluxes and modelled chlorophyll a standing stocks in the Benguela upwelling system. J Mar Syst 180:59–75

Waldron HN, Monteiro PMS, Swart NC (2009) Carbon export and sequestration in the southern Benguela upwelling system: lower and upper estimates. Ocean Sci 5(4):711–718

Wang D, Gouhier TC, Menge BA et al (2015) Intensification and spatial homogenization of coastal upwelling under climate change. Nature 518:390

Wasmund N, Lass HU, Nausch G (2005) Distribution of nutrients, chlorophyll and phytoplankton primary production in relation to hydrographic structures bordering the Benguela-Angolan frontal region. Afr J Mar Sci 27(1):177–190

Weiss RF (1974) Carbon dioxide in water and seawater: the solubility of a non-ideal gas. Mar Chem 2:203–215